Diosmetin blocks type Ⅰ interferon signaling by metabolic control of phosphatidylethanolamine

Nan Shen (nanshensibs@gmail.com)
Shanghai Jiao Tong University School of Medicine https://orcid.org/0000-0002-5875-4417

Xiaoyue Jiang
Shanghai Jiao Tong University School of Medicine

Zhihua Yin
Shenzhen Futian Hospital for Rheumatic Diseases

Can Liu
Shanghai Jiao Tong University School of Medicine

Xingyu Gao
School of Electronic Information and Electrical Engineering, Shanghai Jiao Tong University

Bin Cai
Shanghai Jiao Tong University School of Medicine

Kaixia Zhou
Shanghai Jiao Tong University School of Medicine

Chaojun Qi
Shanghai Jiao Tong University School of Medicine

Jun Deng
Shanghai Jiao Tong University School of Medicine

Bo Qu
Shanghai Jiao Tong University School of Medicine

Yuting Qin
Shanghai Institute of Rheumatology, Renji Hospital, Shanghai Jiao Tong University School of Medicine (SJTUSM), Shanghai

Huihua Ding
Shanghai Institute of Rheumatology, Renji Hospital, Shanghai Jiao Tong University School of Medicine (SJTUSM), Shanghai

Zhizhong Ye
2. Shenzhen Futian Hospital for Rheumatic Diseases, Shenzhen 518040

Lingling Wu
Shanghai Jiao Tong University School of Medicine

Article

Keywords:

Posted Date: February 9th, 2023

DOI: https://doi.org/10.21203/rs.3.rs-2528258/v1

Abstract

Type I interferon (IFN-I) is essential in the development of Systemic Lupus Erythematosus (SLE) and many other autoimmune diseases. To explore the metabolic regulations of IFN-I signaling pathway, we conducted a high through-put screening of a small molecule library and identified diosmetin as a potent compound for blocking IFN-I signaling. We showed diosmetin functioned by preventing the alteration of cellular phosphatidylethanolamine and the spatiotemporal dynamics of IFNAR2 during the activation of IFN-I signaling pathway, and CYP1B1 was verified as the potential target of diosmetin. Further, diosmetin can ameliorate lupus-like autoimmune phenotypes in IFNα-accelerated NZB/NZW F1 lupus model and pristane-induced murine lupus model. Of note, diosmetin can block over-activated IFN-I signaling pathway in PBMCs from lupus patients by reducing the expression of CYP1B1. Our findings reveal a novel lipid metabolic regulation of IFN-I signaling and a potent alternative therapeutic target for autoimmune diseases with overactivated IFN-I signaling pathway.

Introduction

Systemic lupus erythematosus (SLE) is a heterogeneous multi-system autoimmune disease characterized by autoantibody production and innate immune dysfunction[1]. Although significant improvement of the prognosis has been achieved, there are still a lot of patients remain unresponsive to the traditional therapy. It has been documented that type I interferons (IFN-I) are essential in the development of SLE. Compared with healthy controls, elevated expression of multiple interferon-inducible genes, the interferon (IFN) signature, is presented in the peripheral blood cells and damaged organs of SLE patients[2]. It has been shown that the expression level of IFN signature genes predicts disease severity over the next 5 years[3]. Type I interferons are functionally pleiotropic, regulating both innate and adaptive immunity, and involved in a variety of immune disorders in the pathogenesis of SLE, including the differentiation of pro-inflammatory monocytes and the over-activation of autoreactive T and B cells[4]. Therefore, intensive studies have been focusing on developing drugs targeting IFN-I signaling pathway to treat SLE. Encouragingly, FDA has approved anifrolumab, a first-in-class IFN-I receptor blockade, as a novel treatment for SLE[5,6]. Especially, patient subgroups, including IFN score-high patients, patients with abnormal baseline serological markers and Asian patients, had better response to anifrolumab[6]. This reinforces the importance of in-depth study of the molecular regulation of IFN-I signaling pathway. The exploration of more efficient and safer small-molecule compounds targeting new regulatory mechanisms of IFN-I signaling pathway will contribute to the development of novel drugs for SLE[7,8].

Immunometabolism is now considered to play a key role in the pathogenesis of SLE[9,10]. Altered expression of genes controlling metabolism, such as those regulating mitochondrial function, lipid metabolism, and anaerobic glycolysis, has been documented in immune cells of SLE patients or murine lupus models, contributing to the disorder immune status[11–14]. Growing studies have illustrated that metabolites do not only act as intermediates in metabolic processes but also function as critical regulatory molecules in signal transduction[15]. Meanwhile, researches show that inhibition of JAK/STAT

signaling pathway, an important downstream signal transductor for interferon stimulation, can decrease mitochondrial membrane potential, mitochondrial mass, reactive oxygen species, and genes systematically modify lipid metabolism in synovial tissue[16,17]. For example, metabolites such as ATP, lipids, and amino acids may fine-tune IFN-I responses[18]. However, in the current research field, whether there are new metabolic pathways involved in the regulation of the IFN-I pathway which related to the abnormally activated IFN-I in lupus is an unanswered question.

To explore the metabolic regulation mechanisms of IFN-I signaling pathway, we set up a screening platform, based on ISRE-luciferase reporter cell line, and screened 403 small-molecule compounds of a commercial compound library to index their effects on the activation of IFN-I signaling pathway. We identified diosmetin as a potential candidate inhibitor of IFN-I signaling pathway. Since diosmetin is a powerful inhibitor of CYP1B1[19], which participates maintaining cell membrane damage under oxidative stress by lower lipid peroxidation and higher glutathione content[20], we demonstrated that diosmetin negatively regulated IFN-I signaling pathway through affecting phosphatidylethanolamine synthesis. Since intracellular stimulatory signals travel down relies on the property of the phospholipid bilayer of plasma membranes[21],we also demonstrated that diosmetin regulated IFN-I signaling pathway through affected the localization of IFNAR. Furthermore, we demonstrated that systemically administration of diosmetin achieved satisfactory therapeutic effects, in terms of the remission of serological and clinical phenotypes, in type I IFN-accelerated lupus mouse model. What's more, the higher expression of CYP1B1 in PBMCs from lupus patients also indicates a specific role of CYP1B1 in lupus pathology and supports the potential use of diosmetin in treating SLE.

Results

Diosmetin is a novel inhibitor of type I IFN signaling pathway

To explore the metabolic regulation mechanisms of IFN-I signaling, we screened a library of 403 small-molecule compounds with metabolic regulation activity for their effects on ISRE mediated luciferase production using THP1-Dual reporter cells under the stimulation with IFN-I (Fig. 1a). We excluded the compounds with their inhibitory effects were caused by cytotoxicity (Supplementary Fig. 1a). Finally, we found that 77 of the 403 small-molecule compounds had regulatory roles on type I IFN signaling, among which 41 compounds were potential antagonists and 36 compounds were potential agonists. We annotated these compounds, based on public databases and literatures, and found they were regulators of various metabolic pathways with many affected multiple metabolic pathways. Of note, half of the compounds were related to the regulation of lipid metabolism (Fig. 1b).

Among the potential antagonists, we selected diosmetin for further study, because the excellent inhibition effect and safety profile (Fig. 1c). We validated the screening result by showing that diosmetin could reduce the activation of IFN-I signaling pathway in a dose-dependent manner (Fig. 1d) with no obvious

cytotoxicity even at a relatively high dosage (Supplementary Fig. 1b). Consistently, pretreatment of THP-1 cells or human primary monocytes with diosmetin profoundly inhibited the induction of Interferon Stimulated Genes (ISGs), such as ISG15, IFI27, RSAD2, IFI44 (Fig. 2a and 2b). Notably, although less pronounced than in primary monocytes, the repression of IFN-I signaling pathway by diosmetin was also observed in primary T and B cells (Supplementary Fig. 1c, d), which indicates a general mechanism exists behind the inhibitory function of diosmetin on IFN-I signaling. Because we observed stronger inhibitory effects by diosmetin in monocytes and monocytes have a richer expression of ISGs compared with lymphocytes[22], we chose to perform the rest of the experiments mainly in THP-1 cells or human primary monocytes. Besides testing the expression of ISGs, we also examined the activation of crucial signal transducers of IFN-I signaling pathway. We found the levels of the phosphorylation of JAK1 and STAT1 stimulated by IFN-I were significantly downregulated in diosmetin-treated cells (Fig. 2c). Therefore, we identified a novel metabolism regulating compound as a potential antagonist to IFN-I signaling pathway.

Diosmetin prevents the alteration of cellular phosphatidylethanolamine during the activation of type I IFN signaling pathway

To understand the mechanism for the inhibitory effect of diosmetin on the activation of type I IFN signaling pathway, we analyzed the RNA expression profiles of the THP1 cells and the primary monocytes stimulated with IFN-I with or without the presence of diosmetin. We defined the ISGs, using data from THP-1 cells, as genes that were significantly up-regulated by 2-fold after IFN-I stimulation. We found that 314 out of the 433 ISGs were regulated by diosmetin in THP-1 cells; while, 276 ISGs were regulated by diosmetin in primary monocytes, with 211 overlapping genes also existing in THP-1 (Fig. 2d, e, f). The above results not only confirmed our previous findings but also indicated that diosmetin might function by targeting upstream signaling events of type I IFN signaling pathway since we observed a broad inhibition of ISGs.

Diosmetin is involved in regulating cellular metabolism[23], such as fat accumulation and glucose intolerance. In this study, we found that, besides the antiviral genes, genes that were related to lipid metabolism, such as KIR2DL4 and TMEM140, were also differentially expressed under the stimulation of IFN-I (Fig. 2g). Protein-protein interaction network analysis of the differentially expressed genes (DEGs) between IFN-I also showed that there was interaction between lipid metabolism pathways and IFN-I signaling pathway (Fig. 2h). And genes related to lipid metabolism, such as CD93, EPHX4, and SLC40A1, were in the top-ranked DEGs by diosmetin in IFN-stimulated cells (Fig. 2i). Consistently, lipid metabolism pathway was enriched in the DEGs by diosmetin (Fig. 2j). Thus, we wondered whether diosmetin inhibited the activation of type I IFN signaling pathway by acting on lipid metabolism pathways.

To further investigate, we applied targeted metabolomics to profile lipid metabolism in the cells treated with or without diosmetin. 550 lipid metabolites were detected by LC-MS/MS. 403 out of the 550 lipid metabolites were found significantly changed between at least two study groups (Fig. 3a). Additionally, partial least squares discrimination analysis (PLS-DA) revealed that the metabolomic profiles of the four study groups were significantly different (Fig. 3b), indicating distinct lipid metabolism status caused by

different treatments. In THP-1 cells that were only stimulated with type I IFN, 58 differential metabolites had high VIP scores (> 1) by PLS-DA. Out of the 58 metabolites, 27 metabolites belong to phosphatidylcholine (PC) family, and 17 metabolites belong to phosphatidylethanolamine (PE) family (Fig. 3c). While, in the cells stimulated with type I IFN in the presence of diosmetin, 74 differential metabolites had high VIP scores (> 1), out of which 15 metabolites belong to phosphatidylcholine (PC) family, and 18 metabolites belong to phosphatidylethanolamine (PE) family (Fig. 3d). Hierarchical clustering (Fig. 3e) showed that diosmetin prevented IFN-induced lipid metabolism changes. Additionally, star pattern recognition analysis of the six most representative metabolites, including PC (14:0/16:0), PC (14:0/18:0), PC (16:0/16:0), PE (18:0p/18:1), PE (18:0p/16:1) and PE (18:1p/18:1), showed a consistent trend (Fig. 3f), especially for PEs. Furthermore, KEGG analysis of the differential metabolites (Fig. 3g) indicated that glycerophospholipid metabolism pathway was affected by the diosmetin.

Major glycerophospholipids include phosphatidylcholine, phosphatidylethanolamine, phosphatidylserine, phosphatidylinositol, phosphatidylglycerol and phosphatidic acid[24]. Phosphatidylethanolamine (PE) is known to be the second most abundant glycerophospholipid in eukaryotic cells. Since our data suggested that diosmetin prevented the alteration of the abundance of cellular PE during the activation of type I IFN signaling pathway, we examined whether the expression levels of key enzymes of the PE synthesis pathway were affected by diosmetin. We found that the key enzymes in CDP-ethanolamine and phosphatidylserine decarboxylase (Psd) pathways, such as PCYT2, PTDSS1 and PTDSS2, were significantly increased in diosmetin-treated cells (Fig. 3h).

Thus, by analyzing the transcriptome and lipidome, we revealed that the activation of type I IFN signaling pathway altered the cellular phospholipid profile, while diosmetin could prevent the change of phospholipids. These results suggest lipid metabolism may interact with type I IFN signaling pathway and by interfering with the lipid metabolism we may inhibit the activation of type I IFN signaling.

Diosmetin modulates type I IFN signaling by affecting the trafficking of IFNAR2

Previous studies have shown that the relative abundance of various membranous lipids have important effects on the stiffness, thickness, hydrophobicity, and functions of cell membrane[25,26]. For example, de novo synthesis of PE affects the internalization and degradation of CXCR5, which impairs the differentiation of Tfh cells[27]. We have shown that IFN-induced p-JAK1 was reduced by diosmetin, thus diosmetin may affect the activation of IFN-I signaling pathway at the receptor level. Considering that diosmetin prevented the change of PE content during the activation of IFN-I signaling pathway and PE content has been shown associated with the localization of several receptors, we hypothesized diosmetin affected the trafficking of IFNARs after the activation of type I IFN signaling. We found that diosmetin downregulated IFNAR2 at both transcription level (Fig. 4a) and protein level (Fig. 4b). Previous research has shown that receptor dimerization is determined by local receptor concentration for further signaling activation[28]. Thus, we speculated that diosmetin shut down the activation of IFN-I pathway at the very beginning step by reducing the concentration of IFNAR2. Next, confocal images showed that when THP1

cells were unstimulated, the cell membrane boundary was smooth, the thickness of membrane was uniform, and IFNAR2 mainly existed on the cell membrane (Fig. 4c). When THP-1 cells were stimulated by I-IFN, we could see that IFNAR2 was endocytosed and transferred from the cell membrane surface to inner cellular compartment (Fig. 4c, d).Previous study has shown the endocytosis of IFNARs from the outer surface of the cell membrane to the inner cellular compartment is critical for the proper activation of type I IFN signaling[28,29]. Diosmetin restrained the IFNAR2 on the cell membrane, preventing the signal transducing (Fig. 4c, d). Meanwhile, diosmetin prevented the decrease of membranous PE after IFN-I stimulation in THP-1 cells (Fig. 4e, f). We did not see that IFNAR1 was significantly affected in these experiments (Supplementary Fig. 2). These data show that diosmetin could affect type I IFN signaling pathway by modulating the PE levels of plasma membrane and the spatiotemporal dynamics of IFNAR2.

Diosmetin exerts its regulatory effect by targeting CYP1B1

To further explore the specific protein targets of diosmetin, we unearthed 10 candidate targets in Stich database by virtual algorithm, including CYP1B1, CYP2J2, CYP2U1, CYP2R1, ABCC3 and five other unannotated proteins, among which CYP1B1 acquired the highest predictive score (Supplementary Fig. 3a, 3b). Besides, we carried out molecular docking[30,31] to simulate the binding of above five annotated proteins to diosmetin respectively. We found 6IQ5 as the active site on CYP1B1 protein with the highest Libscore (Fig. 5a, 5b). Additionally, we re-analyzed the expression of the above predicted targets in the RNA-seq data previously described in this study and found that diosmetin reduced CYC1B1 mRNA expression levels in THP-1 cells (Supplementary Fig. 3c) and in CD14 + monocytes (Supplementary Fig. 3d) significantly, but not affecting other predicted candidates. We also verified above findings at both transcription level (Fig. 5c) and the protein level (Fig. 5d) in THP-1.In addition, protein-protein interaction analysis also suggested interactions between the interferon pathway, lipid metabolism, and cytochrome P450-related proteins, eg, CYP1B1, CYP7A1, CYP2C18, and CYP2C19 (Supplementary Fig. 3e, 3f). Of note, in THP1 cells, after knockdown of CYP1B1, the ISGs (RSAD2, IFIT3, and IFI44) were all down-regulated as expected (Fig. 5e).Vice versa, overexpression of CYP1B1 could upregulate the induction of ISGs by I IFN (Fig. 5f). Further, because CYP1B1 was reported to be involved in an NADPH-dependent electron transport pathway ($RH + NADPH + H + O2 \rightarrow ROH + NADP + H20$)[32–34]. We found that the intracellular function of CYP1B1 was indeed inhibited by diosmetin (Supplementary Fig. 3g-3j). These data suggest that CYP1B1 is a bona fide target of diosmetin modulating type I IFN signaling pathway.

Diosmetin can alleviate lupus-like phenotypes in IFNa-accelerated NZB/NZW F1 lupus mouse model

Since blocking the activation of type I IFN signaling pathway can be used to treat SLE, we further tested if diosmetin could alleviate the lupus-like phenotypes in IFNa-accelerated NZB/NZW F1 lupus mouse model (Fig. 6a). Diosmetin was administered by intraperitoneal injections(50mg/kg)every other day. We did not observe any significant changes of the body weights or the transaminase levels in diosmetin treated mice, indicating the regime was safe (Supplementary Fig. 5a-5c). We found that diosmetin significantly reduced the mortality of the lupus mice (Fig. 6b), as well as improved lupus phenotypes including

proteinuria (Fig. 6c), anti-dsDNA autoantibody titers in serum (Fig. 6d), renal pathology scores (Fig. 6e), and the deposition of C3 and immune complexes in renal tissue (Fig. 6f). At the same time, the expression levels of ISGs in the kidney were also significantly downregulated compared to vehicle treatment (Fig. 6g). Moreover, RNA-seq profiling revealed that most ISGs in kidney were also significantly downregulated by diosmetin in spontaneous NZB/NZW F1 lupus mice (Supplementary Fig. 4a). Of note, we examined the expression of CYP1B1 protein levels in kidney and found that CYP1B1 protein was mainly localized in damaged glomeruli, such as areas of glomerular thickening or lobular segmentation. After treatment with diosmetin, the expression level of CYP1B1 was significantly decreased as well as the reduction of glomerular lesions, indicating that diosmetin exerted its effect through regulating CYP1B1 (Fig. 6h). We also analyzed the expression levels of the key enzymes involved in the phosphatidylethanolamine biosynthetic pathway in our lupus mouse kidney RNA-seq data and obtained results consistent with the previous in vitro experiments (Supplementary Fig. 4b). The above results were repeated in another induced lupus mouse model, and diosmetin showed the same therapeutic effect (Supplementary Fig. 5d-5i).

Besides the animal model data, we also conducted experiments in primary cells from lupus patients. First, the expression of CYP1B1 was dramatically elevated in the PBMCs from SLE patients, and treatment with diosmetin reduced the overexpression of CYP1B1 to the normal level (Fig. 7a). Second, diosmetin reduced the ISGs' expression significantly as compared to control group (Fig. 7b). Interestingly, diosmetin acted only on the cells from patients with high IFN score, but not on cells from patients with low IFN score (Fig. 7c). The above results suggest that diosmetin is a possible treatment for lupus patients with high IFN scores.

Discussion

SLE remains a challenging autoimmune disease to treat due to the heterogeneity of disease manifestations and treatment response. Overactivated type I IFN signaling has been associated with SLE initiation[2,3,35]. Meanwhile, a Mendelian form of SLE caused by ACP5 mutations suggests that an upregulation of type I IFN signaling may serve as a defining feature of autoimmunity disease[36]. Previous researchers have found that rIFN-α2a treatment on patients with chronic hepatitis C causes substantial changes in serum lipoprotein metabolism[37]. Chronic IFN-I stimulation accelerates terminal CD8 + T cell exhaustion by inducing lipid peroxidation[38]. Exposure of bone marrow–derived macrophages to IFN-β suppressed the synthesis of saturated and unsaturated long-chain fatty acids and cholesterol while increasing the import of fatty acids and cholesterol[39]. Above evidences show IFN-I influences the lipid metabolism of immune cells which may play a significant role in patients with SLE[9,10,40]. Of note, $CD4^+$ T cells from SLE patients have significantly elevated lipid raft-associated glycosphingolipids which lead to abnormal T-cell receptor signaling[41]. These studies promote us to further investigate the crosstalk between the over-activation of IFN-I and the abnormal lipid metabolism in SLE patients. Our study firstly presents the change of lipidomes in monocytes after IFN-I stimulation. Besides, we have identified a novel

small molecule compound, Diosmetin, preventing the lipidomic change in IFN-I stimulated monocytes, and blocking the subsequential activation of IFN-I signaling.

Type I IFN signaling is regulated in a quantitative and qualitative manner[42]. Lots of studies have focused on how the signaling is amplified by the induction of STAT1 and IRF9 expression. But few studies focused on the qualitative aspect of IFN-I signaling, such as the proper distribution of IFNARs. In 2006, the Lamaze group revealed for the first time that IFNAR endocytosis was required to trigger JAK/STAT signaling downstream of IFN-a stimulation, which raised the question that how IFNAR trafficking in cellular compartments affected the proper activation of IFN-I signaling[43]. Our research firstly demonstrated diosmetin could prevent the change of phospholipids caused by IFN-I. Thus, diosmetin altered the plasma membrane integrity and blocked the signaling transduction by interfering the endocytosis of IFNAR2.

Diosmetin is a mono-methoxy flavone, which is a natural substance isolated from citrus fruits[44]. It is reported to exhibit anticancer, antimicrobial, antioxidant, oestrogenic and anti-inflammatory activities[19,44,45]. Interestingly, researchers find that flavonoids might serve as a treatment for the thrombotic complications implicated in COVID-19[46]. Most of these studies have been carried out through in vitro and in silico models, and limited studies have reported the in vivo and clinical effects of flavonoids. In our study, diosmetin safely and effectively alleviated the lupus-like phenotypes in IFNa-accelerated NZB/NZW F1 lupus mouse model, which expands its potential indications to autoimmune diseases related to abnormal IFN-I signaling activation such as SLE and interferonopathy.

Previous report described cytochrome P450 CYP1 enzymes as the possible target of diosmetin[19]. In our research, we identified CYP1B1 as the specific target by performing molecular docking, then validated the predicted results by loss and gain of function study. CYP1B1 is one of the major P450 isoenzyme, which widely expressed in many organs and immune cells[47]. CYP1B1 deficiency lead to impaired macrophage function[48]. Moreover, CYP1B1 was reported to be involved in an NADPH-dependent electron transport pathway ($RH + NADPH + H + O2 \rightarrow ROH + NADP + H20$)[32–34], which is vital for physiological function of plasma membrane[49–51]. For example, a recent study illustrated that NADPH-cytochrome P450 reductase (POR) and NADH-cytochrome b5 reductase (CYB5R1) transfer electrons from NAD(P)H to oxygen to hydrogen peroxide generation, resulting in disrupting membrane integrity during ferroptosis[52]. In our study, we found that the expression of CYP1B1 was elevated in the PBMCs from lupus patients and it can also be induced by IFN-I in monocytes. Based on above findings, we speculate that the increase of CYP1B1 might enhance the electron transport pathway, thus consuming more hydrogen ions and changing the intracellular pH value. The transmembrane pH gradients might induce lipid asymmetry[53], which might ultimately affect the localization of IFNAR2 and the activation of downstream signaling. Thus, we raised a novel model for regulating IFN-I pathway in both quantitative and qualitative manner. As a positive feedback regulator, CYP1B1, which induced by IFN-I, amplifies IFN-I signaling pathway by affecting the spatial distribution of IFNAR2 (Fig. 8). The exact mechanism by which the alteration of

cellular lipidome stimulated by IFN-I contributes to the activation of IFN-I signaling pathway and how this mechanism is involved in lupus pathogenesis need further exploration.

In our study, we observed a high expression of CYP1B1 in the PBMCs from SLE patients. And the expression of CYP1B1 protein was mainly localized in damaged glomeruli of kidney tissues from lupus mice model. These findings first proved that CYP1B1 might play a role in the progression of SLE, which supported the subsequential pre-clinical study of diosmetin in lupus mice model.

In conclusion, we proposed a novel molecular regulatory mechanism of IFN-I pathway, clarified the significant role of phospholipid metabolism in IFN-I signaling activation, and identified a small molecule compound that inhibits IFN-I pathway by the above mechanism. What's more, the efficacy of diosmetin in the lupus mouse model with excessive activation of IFN-I proves the prospect of further clinical application of this newly identified small molecule compound.

Methods

Human subjects A total of 34 PBMCs from patients of SLE and 16 healthy controls were from Ren Ji Hospital Biobank of Shanghai Jiao Tong University School of Medicine. The study was approved by the Research Ethics Board of Ren Ji Hospital. Signed Informed Consent Forms were collected from all subjects. All enrolled SLE patients were diagnosed recording to SLICC criteria for SLE in 2012[54,55], or 2019 EULAR/ACR criteria[56]. The demographic clinical information of the subjects was listed in Supplementary Table 1–3.

Mice. C57BL/6N mice were purchased from Vital River Laboratories. Female NZB/BINJ mice and male NZW/LacJ mice were purchased from The Jackson Laboratory. NZB/NZW F1 mice were produced by hybridizing crosses between female NZB/BINJ mice and male NZW/LacJ mice. All animals were maintained in a specific pathogen-free facility at Shanghai Rat&Mouse Biotech Company in a 12-h light/12-h dark cycle and free acquirement to sterile water and a standard mouse diet. Animal studies were approved by the Institutional Animal Care and Use Committee at Ren Ji Hospital, Shanghai Jiao Tong University School of Medicine.

For ex vivo assessment of the effect of Diosmetin on I IFN signaling, 8 weeks old female C57BL/6N mice were intraperitoneally administrated with Diosmetin (50mg/kg) or vehicles for 48 hours, then splenocytes from these mice were stimulated with 1000 U/ml of universal type I IFN (R&D System).

To evaluate the therapeutic effects of diosmetin, 6 weeks old female NZB/NZW F1 mice were intravenously injected with 10^9 pfu of IFNa5-encoding adenovirus particles (ViGene Biosciences). After 6 weeks, mice were randomized and grouped regarding their urinary protein levels. These mice were intraperitoneally administrated with diosmetin (50mg/kg, Selleck Chemicals) or vehicles every other day for continuous treatment cycles of 6 weeks. TMPD induced lupus mice model was created by intraperitoneally injecting C57BL/6N mice with 0.5 ml TMPD once (0.783g/ml, Sigma). Five months later, diseased mice were randomly divided into two groups accepting diosmetin or vehicle treatment.

Peripheral blood from above mice was collected in tubes containing ethylenediaminetetraacetic acid to isolate plasma. Anti-dsDNA autoantibody was detected with Mouse anti-dsDNA IgG-specific ELISA Kit (Alpha Diagnostic International), anti-ANA autoantibody was detected with Mouse anti-ANA ELISA Kit (Alpha Diagnostic International). To evaluate the hepatotoxicity of diosmetin, plasma ALT and AST level were measured separately with Mouse ALT or AST ELISA Kit (Alan Transaminase, FineTest). At a specific time point, mice were kept in separate metabolic cages for 24 hours, and the urine was collected to evaluated the kidney damage of lupus mice. Urinary protein was detected by BCA Protein Assay Kit (TIANGEN).

Cell culture THP-1 cells (Cell Bank, Shanghai Institutes for Biological Science, Chinese Academy of Sciences) were cultured in RPMI 1640 medium supplied with 10% (v/v) fetal bovine serum (Gibco), 2 mM L-Glutamine, 1mM sodium pyruvate and 10 mM HEPES at 37℃ in a cell incubator containing 5% CO_2. PBMCs were collected by using Ficoll-Paque PLUS (Citiva) according to manufacturer's instructions. CD14 + monocytes were separated from PBMCs via magnetic beads sorting (Miltenyi Biotech), and the purity (> 98%) was verified by anti-CD14 antibody (BD biosciences) through flow cytometry (BD FORTESSA). THP-1 cells or primary monocytes were pretreated with 50 uM Diosmetin or vehicle for 30 minutes, then type I IFN 1000 U/ml was added. PBMCs from patients of SLE were incubated with Diosmetin 50 uM or vehicle for 3 hours. Cells were collected to extract RNA or protein for downstream analysis.

For transient transfection, THP-1 cells ($2*10^5$/well) were cultured in a 24-well plate for 24 hours, and siRNAs (200uM) targeting CYP1B1 were transfected into THP-1 cells with LipofectamineTM RNAiMAX (Invitrogen). 24 hours later, cells were stimulated with type IFN-I (1000 U/ml) and harvested at indicated timepoint for further analysis. The sequences of all siRNAs (RIBOBIO Biotech) are in Supplementary Table 4.

For stable transfection, hsa-CYP1B1 (transcripts NM_000104.4) was constructed into pLV6ltr-ZsGreen-Puro-CMV (TSINGKE), the modified plasmid was transfected into 293T cells together with package plasmids (TSINGKE). The virus supernatant was collected for concentration and titrated to 5E + 8TU/mL. Lentiviruses that carried CYP1B1 or negative control were respectively added to THP-1 cells at MOI 50. After 72h, THP-1 cells stably expressing CYP1B1 were sorted by flow cytometry (BD AIRA, BD biosciences).

For NADP + and NADPH quantification, THP-1 cells, THP1-NC and THP1-CYP1B1 cells were individually pretreated with 50 uM Diosmetin or vehicle for 30 minutes, then type I IFN 1000 U/ml was added for the designated time. Then each sample was harvested and resuspended by 200 μL NADP+/ NADPH extraction solution (Beyotime, China), the extracts were centrifuged at 12000 g for 10 min at 4°C to collect the supernatant. The supernatant was added to the 96 well plates with G6PDH working solution and incubated at 37°C for 10 min. Then the absorbance was read at 450 nm absorbance to calculate the total quantity of NADP + and NADPH. Next, NADP + was water bath inactivated at 60°C for 30 min. And the supernatant was measured as above to calculate the quantification of NADPH.

For the measurement of intracellular pH (ipH), THP-1 cells were pretreated with 50 uM Diosmetin or vehicle for 30 minutes, then type I IFN 1000 U/ml was added. And cells were harvested and washed twice with PBS (Ca^{2+} -free, Mg^{2+}-free, PH = 7.4, BasalMedia, Shanghai), then cells were incubated in PBS containing 2 μM BCECF-AM, a fluorescent probe that binds specifically to hydrogen ions, for 30 min at 37°C in 5% humidified CO2. Next, cells were then washed with PBS three times. The ipH level was measured by the mean fluorescence intensity through flow cytometry (BD FORTESSA) with an excitation wavelength 488nm and an emission wavelength 535nm.

Hematoxylin and eosin (H&E) staining, IHC assay and immunofluorescence staining of kidney tissue. Kidneys from lupus mice model were fixed in 4% formaldehyde solution immediately after the mice were sacrificed. Then the fixed tissue were embedded in paraffin and 5 um thickness sections were made and stained with hematoxylin and eosin (H&E). Blinded assessment of renal pathological scores was performed by a senior renal pathologist, as previously described [57].

For IHC assay, sections above proceeded to deparaffinization and hydration. Antigen was retrieved in citrate buffer (0.01 M, pH 6.0) at 95°C for 10 min, and then the sections were incubated with blocking buffer (5% BSA in PBS) for 60 min at room temperature, stained with anti-CYP1B1 (ABclonal Technology) at 4°C overnight. On day 2, sections were incubated with secondary antibody. Then the slides were incubated with secondary antibody at the second day before incubating with DAB and DAB buffer (1:19 mixture) for 10 minutes (Dako REAL™ EnVision™ Detection System). Slides were counterstained for 5 minutes with Schmidt hematoxylin, followed by several rinses with wash buffer and distilled water. Subsequently, slides were dehydrated with increasing concentrations of ethanol and cleared with xylene. At last, the image was recorded by Nikon Eclipse Ci-L microscope. The proportion of areas staining positive for CYP1B1 was quantified by IHC profiler plugin in ImageJ (NIH image program, version 2.9.0). Immune complexes precipitation in the glomerulus is stained by immunofluorescence with anti-mouse IgG2a (Santa Cruz Biotechnology) and anti-mouse C3 (Abcam). The immunofluorescence was assessed by TissueFAXS Viewer software.

Cellular immunofluorescence staining. Cells were collected and washed with PBS to remove stimuli, then cells were stained with DiOC18(3) (3,3'-dioctadecyloxacarbocyanine perchlorate) (Cell Plasma Membrane Staining Kit ,Beyotime). Then, cells were fixed and permeabilized by BD Cytofix/Cytoperm™ kit (BD Bioscience). Next, the cells were blocked by 10% FBS for 30 minutes, then they were individually incubated by primary antibody IFNAR1/IFNAR2/CYP1B1 (ABclonal Technology) and duramycin-LC-biotin (Molecular Targeting Technologies) at 4 ℃ overnight. On day 2, the secondary antibody Cy3 Goat Anti-Rabbit IgG (H + L) (ABclonal Technology) and APC-conjugated streptavidin (BD Bioscience) were added. Finally, for nuclear staining, DAPI (1:5000) (BD Bioscience) was incubated for 10 minutes. Images of cells were acquired by the confocal microscope (Leica, SP8). ImageJ software with plugin JACoP47 and RGB Profiler were applied to analyze the fluorescence intensity in marked regions, calculate the Manders' coefficient and quantify the RGB intensity[58].

Quantification of Gene Expression. Total RNA was extracted with TRIzol reagent (Invitrogen), then RNA was synthesized to complementary DNA with PrimeScript RT Reagent Kit (Takara Bio). The expression of different genes was quantified with SYBR Premix Ex Taq Kit (Takara Bio). Then genes were amplified on a QuanStudio 7 Flex Real-Time PCR System (Applied Biosystems). The expression of genes was normalized to RPL13a by the 2-△△Ct value. All primers are listed in Supplementary Table 5.

Immunoblotting. Cells were collected and lysed in RIPA Lysis Buffer supplemented with Halt™ Protease and Phosphatase Inhibitor Cocktail (Thermo Fisher Scientific). Individual cell lysates with 10 ug/lane were separated by 10% SDS PAGE and then transferred to PVDF membranes (Millipore). Next, the membranes were blocked by BSA buffer (Sangon Biotech). Targeted proteins were detected by corresponding primary antibodies and corresponding secondary peroxidase-conjugated antibodies. The antibodies used in the study are listed in Supplementary Table 6. Finally, bands were detected by Pierce ECL Western Blotting Substrate (Thermo Fisher Scientific). Images were captured by Tanon 5500 Imaging System and measured by ImageJ software.

Gene expression profiling. THP-1 cells were collected and proceeded to RNA extraction with TRIzol reagent. RNA integrity was evaluated using the Agilent 2100 Bioanalyzer (Agilent Technologies, Santa Clara, CA, USA). The samples with RNA Integrity Number (RIN) ≥ 7 were quality acceptable and subjected to the subsequent sequencing. The libraries were constructed with TruSeq Stranded Total RNA with Ribo-Zero Gold. These libraries were then sequenced on the Illumina sequencing platform (HiSeqTM 2500 or other platforms) and fragments with 150/125 bp paired-end reads were obtained. Differential screening analysis and functional analysis were proceeded by estimateSizeFactors function of the DESeq R package to normalize the counts and then by nbinomTest function analysis to calculate the P-value and fold change values for the difference comparison. Transcripts with p-values < = 0.05 and fold change > = 2 were selected. Analysis of differential mRNA GO and KEGG enrichment is by Hypergeometric Distribution Test.

LC–MS lipid profiling and data processing. Celluar samples were collected in liquid nitrogen immediately and proceeded a modified Folch lipid extraction procedure. Subsequently, above samples were analysed by LC-MS/MS lipid profiling. LC separations was performed on ExionLC™ System and MS was QTRAP® 6500+ (Sciex, USA) equipped with an IonDriveTM Turbo V source.

A total of 15 kinds of glycerophospholipids, glycerolipids, and sphingolipids isotope-labeled internal mix standards were from Avanti Polar Lipids (Birmingham, AL, USA), Palmitic acid-16,16,16-d3, Stearic acid-18,18,18-d3, and different Acyl carnitine-d3 were purchased from Sigma-Aldrich (St. Louis, MO, USA). All organic solvents and water used in sample and mobile phase preparations were HPLC grade and obtained from Fisher Scientific (Fair Lawn, NJ, USA).

The raw data generated by LC-MS/MS was first evaluated by QC sample. Qualified samples were further processed using MRMPROBS software to perform peak integration, calibration, and quantitation for each lipid. Data matrix of lipids was further analyzed on MetaboAnalyst 5.0. Partial Least Sequences-Discriminant Analysis (PLS-DA) was used to identify the important features in different groups.

Importance in Projection (VIP) is a weighted sum of squares of the PLS loadings taking into account the amount of explained Y-variation in each dimension. VIP score id calculated for each component. When more than one component is used to calculate the feature importance, the average of the VIP scores is used. The other important measure of PLS-DA is the weighted sum of PLS-regression.

For star pattern recognition and statistical analysis, the concentration of three phosphatidylcholines (PC) and three phosphatidylethanolamines (PE) were detected by LC-MS/MS lipid profiling. Then, the quantitative level of each PC and PE was normalized to the corresponding mean value of DMSO group. These normalized values were then used to draw star graphs.

Molecular docking. The molecular docking studies were carried out between diosmetin and five potential ligands predicted by the STITCH database (http://http://stitch.embl.de/). The 2D structure of diosmetin and selected ligands was obtained from the PubChem database (https://pubchem.ncbi.nlm.nih.gov/), then it was transferred to the 3D structure by Chem 3D 19.0 software. All bound substances (ligands and cofactors) and water molecules associated with the receptor were removed before in silico docking process. The prepared ligands were docked with the prepared structure of diosmetin using Discovery Studio 2019 software. The docking results were evaluated by Libscores which were generated in the software.[31]

Statistical analysis. Results were analyzed and figures were generated with GraphPad Prism (Version 9.0.0). The corresponding nonparametric Mann-Whitney U-test, Spearman's correlation test, Student's paired t-test, two-way ANOVA, and log-rank test were applied according to different data types. A significant difference was considered when the P value was < 0.05.

Declarations

Acknowledgments

We thank all members of Shen's lab for sharing reagents, comments and support to this project. The work was supported by Shanghai Pujiang Program (21PJD037), National Natural Science Foundation of China (No. 31930037, No. 32141004, No. 32170903, No.82001709), Shanghai Science and Technology Innovation Plan (21Y31900200) and Sanming Project of Medicine in Shenzhen (SZSM201602087).

Author contributions

N.S. and L.W. designed this study, organized the experiments, and supervised the project. X.J. and C.L. performed most of the experiments. L.W and X.J. wrote the manuscript. N.S. supervised the manuscript. C.L. and Z.Y. collected the clinical samples. H.D. analyzed the data from clinical samples.X.J., L.W., and X.G. performed bioinformatic analysis. C.J. helped evaluated renal pathological histology. J.D., Y.Q., X.G., B.C., Z.Y., C.J., and B.Q. provided conceptual advice or supervised a specific part of experiments. N.S. and L.W. directed data analysis and graphic presentation form and finalized the manuscript. All authors critically read and brought forward their opinions on the final manuscript.

Competing interests

The authors declare no competing interests.

References

1. Tsokos, G. C., Lo, M. S., Reis, P. C. & Sullivan, K. E. New insights into the immunopathogenesis of systemic lupus erythematosus. Nature Reviews Rheumatology **12**, 716–730, doi:10.1038/nrrheum.2016.186 (2016).
2. Nikpour, M., Dempsey, A. A., Urowitz, M. B., Gladman, D. D. & Barnes, D. A. Association of a gene expression profile from whole blood with disease activity in systemic lupus erythaematosus. Ann Rheum Dis **67**, 1069–1075, doi:10.1136/ard.2007.074765 (2008).
3. Mai, L. *et al.* The baseline interferon signature predicts disease severity over the subsequent 5 years in systemic lupus erythematosus. Arthritis Research & Therapy **23**, 9, doi:10.1186/s13075-021-02414-0 (2021).
4. Barrat, F. J., Crow, M. K. & Ivashkiv, L. B. Interferon target-gene expression and epigenomic signatures in health and disease. Nature Immunology **20**, 1574–1583, doi:10.1038/s41590-019-0466-2 (2019).
5. Mullard, A. FDA approves AstraZeneca's anifrolumab for lupus. Nature Reviews Drug Discovery **20**, 658–658 (2021).
6. Vital, E. M. *et al.* Anifrolumab efficacy and safety by type I interferon gene signature and clinical subgroups in patients with SLE: post hoc analysis of pooled data from two phase III trials. Annals of the Rheumatic Diseases **81**, 951–961, doi:10.1136/annrheumdis-2021-221425 (2022).
7. Dörner, T. & Furie, R. Novel paradigms in systemic lupus erythematosus. The Lancet **393**, 2344–2358, doi:https://doi.org/10.1016/S0140-6736(19)30546-X (2019).
8. Parra Sánchez, A. R., Voskuyl, A. E. & van Vollenhoven, R. F. Treat-to-target in systemic lupus erythematosus: advancing towards its implementation. Nat Rev Rheumatol **18**, 146–157, doi:10.1038/s41584-021-00739-3 (2022).
9. Sharabi, A. & Tsokos, G. C. T cell metabolism: new insights in systemic lupus erythematosus pathogenesis and therapy. Nature Reviews Rheumatology **16**, 100–112, doi:10.1038/s41584-019-0356-x (2020).
10. Takeshima, Y., Iwasaki, Y., Fujio, K. & Yamamoto, K. Metabolism as a key regulator in the pathogenesis of systemic lupus erythematosus. Seminars in Arthritis and Rheumatism **48**, 1142–1145, doi:https://doi.org/10.1016/j.semarthrit.2019.04.006 (2019).
11. Jaroonwitchawan, T. *et al.* Dysregulation of Lipid Metabolism in Macrophages Is Responsible for Severe Endotoxin Tolerance in FcgRIIB-Deficient Lupus Mice. Frontiers in Immunology **11**, 21, doi:10.3389/fimmu.2020.00959 (2020).
12. He, J. *et al.* Microbiome and Metabolome Analyses Reveal the Disruption of Lipid Metabolism in Systemic Lupus Erythematosus. Frontiers in Immunology **11**, doi:10.3389/fimmu.2020.01703 (2020).

13. Li, H., Meng, D., Jia, J. & Wei, H. PGLYRP2 as a novel biomarker for the activity and lipid metabolism of systemic lupus erythematosus. Lipids in health and disease **20**, 95–95, doi:10.1186/s12944-021-01515-8 (2021).
14. Morel, L. Immunometabolism in systemic lupus erythematosus. Nature Reviews Rheumatology **13**, 280–290, doi:10.1038/nrrheum.2017.43 (2017).
15. Wang, X. *et al.* α-Ketoglutarate-Activated NF-κB Signaling Promotes Compensatory Glucose Uptake and Brain Tumor Development. Mol Cell **76**, 148–162.e147, doi:10.1016/j.molcel.2019.07.007 (2019).
16. McGarry, T. *et al.* JAK/STAT Blockade Alters Synovial Bioenergetics, Mitochondrial Function, and Proinflammatory Mediators in Rheumatoid Arthritis. Arthritis Rheumatol **70**, 1959–1970, doi:10.1002/art.40569 (2018).
17. Robinson, G., Pineda-Torra, I., Ciurtin, C. & Jury, E. C. Lipid metabolism in autoimmune rheumatic disease: implications for modern and conventional therapies. J Clin Invest **132**, doi:10.1172/jci148552 (2022).
18. Ahmed, D. & Cassol, E. Role of cellular metabolism in regulating type I interferon responses: Implications for tumour immunology and treatment. Cancer Letters **409**, 20–29, doi:10.1016/j.canlet.2017.08.037 (2017).
19. Androutsopoulos, V. P., Papakyriakou, A., Vourloumis, D., Tsatsakis, A. M. & Spandidos, D. A. Dietary flavonoids in cancer therapy and prevention: Substrates and inhibitors of cytochrome P450 CYP1 enzymes. Pharmacology & Therapeutics **126**, 9–20, doi:https://doi.org/10.1016/j.pharmthera.2010.01.009 (2010).
20. Villa, P. *et al.* Protective effect of diosmetin on in vitro cell membrane damage and oxidative stress in cultured rat hepatocytes. Toxicology **73**, 179–189, doi:https://doi.org/10.1016/0300-483X(92)90101-J (1992).
21. Ivanova, P. T., Milne, S. B., Forrester, J. S. & Brown, H. A. LIPID arrays: new tools in the understanding of membrane dynamics and lipid signaling. Mol Interv **4**, 86–96, doi:10.1124/mi.4.2.6 (2004).
22. Han, S. H. *et al.* Differential Responsiveness of Monocyte and Macrophage Subsets to Interferon. Arthritis & Rheumatology **72**, 100–113, doi:10.1002/art.41072 (2020).
23. Chung, S., Kim, H.-J., Choi, H.-K., Park, J. H. & Hwang, J.-T. Comparative study of the effects of diosmin and diosmetin on fat accumulation, dyslipidemia, and glucose intolerance in mice fed a high-fat high-sucrose diet. Food Science & Nutrition **8**, 5976–5984, doi:https://doi.org/10.1002/fsn3.1883 (2020).
24. Calzada, E., Onguka, O. & Claypool, S. M. Phosphatidylethanolamine Metabolism in Health and Disease. Int Rev Cell Mol Biol **321**, 29–88, doi:10.1016/bs.ircmb.2015.10.001 (2016).
25. Umebayashi, M. *et al.* A covalently linked probe to monitor local membrane properties surrounding plasma membrane proteins. Journal of Cell Biology **222**, doi:10.1083/jcb.202206119 (2022).
26. Kalxdorf, M. *et al.* Cell surface thermal proteome profiling tracks perturbations and drug targets on the plasma membrane. Nature Methods **18**, 84–91, doi:10.1038/s41592-020-01022-1 (2021).

27. Fu, G. *et al.* Metabolic control of T(FH) cells and humoral immunity by phosphatidylethanolamine. Nature **595**, 724–729, doi:10.1038/s41586-021-03692-z (2021).
28. Schreiber, G. & Piehler, J. The molecular basis for functional plasticity in type I interferon signaling. Trends in Immunology **36**, 139–149, doi:https://doi.org/10.1016/j.it.2015.01.002 (2015).
29. Zanin, N., Viaris de Lesegno, C., Lamaze, C. & Blouin, C. M. Interferon Receptor Trafficking and Signaling: Journey to the Cross Roads. Front Immunol **11**, 615603, doi:10.3389/fimmu.2020.615603 (2020).
30. Li, Y. *et al.* Assessing protein-ligand interaction scoring functions with the CASF-2013 benchmark. Nat Protoc **13**, 666–680, doi:10.1038/nprot.2017.114 (2018).
31. Adeniji, S. E., Uba, S. & Uzairu, A. In silico study for evaluating the binding mode and interaction of 1, 2, 4-triazole and its derivatives as potent inhibitors against Lipoate protein B (LipB). Journal of King Saud University - Science **32**, 475–485, doi:https://doi.org/10.1016/j.jksus.2018.07.014 (2020).
32. Catala, A., Zvara, A., Puskas, L. G. & Kitajka, K. Melatonin-induced gene expression changes and its preventive effects on adriamycin-induced lipid peroxidation in rat liver. Journal of Pineal Research **42**, 43–49, doi:10.1111/j.1600-079X.2006.00354.x (2007).
33. Le, T. K. *et al.* Solar-Powered Whole-Cell P450 Catalytic Platform for C-Hydroxylation Reactions. *ChemSusChem* **14**, 3054–3058, doi:10.1002/cssc.202100944 (2021).
34. Liu, Q. L. *et al.* Bioinformatic analysis of gene expression profile in prostate epithelial cells exposed to low-dose cadmium. International Journal of Clinical and Experimental Medicine **11**, 1669–1678 (2018).
35. Muskardin, T. L. W. & Niewold, T. B. Type I interferon in rheumatic diseases. Nat Rev Rheumatol **14**, 214–228, doi:10.1038/nrrheum.2018.31 (2018).
36. Briggs, T. A. *et al.* Tartrate-resistant acid phosphatase deficiency causes a bone dysplasia with autoimmunity and a type I interferon expression signature. Nature Genetics **43**, 127–131, doi:10.1038/ng.748 (2011).
37. Shinohara, E. *et al.* Interferon α induces disorder of lipid metabolism by lowering postheparin lipases and cholesteryl ester transfer protein activities in patients with chronic hepatitis C. Hepatology **25**, 1502–1506, doi:https://doi.org/10.1002/hep.510250632 (1997).
38. Chen, W. *et al.* Chronic type I interferon signaling promotes lipid-peroxidation-driven terminal CD8 + T cell exhaustion and curtails anti-PD-1 efficacy. Cell Reports **41**, 111647, doi:https://doi.org/10.1016/j.celrep.2022.111647 (2022).
39. York, Autumn G. *et al.* Limiting Cholesterol Biosynthetic Flux Spontaneously Engages Type I IFN Signaling. Cell **163**, 1716–1729, doi:https://doi.org/10.1016/j.cell.2015.11.045 (2015).
40. Teng, X., Brown, J., Choi, S. C., Li, W. & Morel, L. Metabolic determinants of lupus pathogenesis. Immunol Rev **295**, 167–186, doi:10.1111/imr.12847 (2020).
41. McDonald, G. *et al.* Normalizing glycosphingolipids restores function in CD4 + T cells from lupus patients. The Journal of Clinical Investigation **124**, 712–724, doi:10.1172/JCI69571 (2014).

42. Ivashkiv, L. B. & Donlin, L. T. Regulation of type I interferon responses. Nature Reviews Immunology **14**, 36–49, doi:10.1038/nri3581 (2014).
43. Marchetti, M. *et al.* Stat-mediated signaling induced by type I and type II interferons (IFNs) is differentially controlled through lipid microdomain association and clathrin-dependent endocytosis of IFN receptors. Mol Biol Cell **17**, 2896–2909, doi:10.1091/mbc.e06-01-0076 (2006).
44. Hostetler, G. L., Ralston, R. A. & Schwartz, S. J. Flavones: Food Sources, Bioavailability, Metabolism, and Bioactivity. Advances in Nutrition **8**, 423–435, doi:10.3945/an.116.012948 (2017).
45. Liu, B. *et al.* Diosmetin induces apoptosis by upregulating p53 via the TGF-β signal pathway in HepG2 hepatoma cells. Mol Med Rep **14**, 159–164, doi:10.3892/mmr.2016.5258 (2016).
46. Quintal Martínez, J. P. & Segura Campos, M. R. Flavonoids as a therapeutical option for the treatment of thrombotic complications associated with COVID-19. *Phytotherapy Research* **n/a**, doi:https://doi.org/10.1002/ptr.7700.
47. Li, F., Zhu, W. & Gonzalez, F. J. Potential role of CYP1B1 in the development and treatment of metabolic diseases. Pharmacol Ther **178**, 18–30, doi:10.1016/j.pharmthera.2017.03.007 (2017).
48. Ward, J. M. *et al.* Progressive glomerulonephritis and histiocytic sarcoma associated with macrophage functional defects in CYP1B1-deficient mice. Toxicol Pathol **32**, 710–718, doi:10.1080/01926230490885706 (2004).
49. Shi, T. *et al.* Nanohole-boosted electron transport between nanomaterials and bacteria as a concept for nano-bio interactions. Nature communications **12**, 493–493, doi:10.1038/s41467-020-20547-9 (2021).
50. Vercellino, I. & Sazanov, L. A. The assembly, regulation and function of the mitochondrial respiratory chain. Nature Reviews Molecular Cell Biology **23**, 141–161, doi:10.1038/s41580-021-00415-0 (2022).
51. Letts, J. A. & Sazanov, L. A. Clarifying the supercomplex: the higher-order organization of the mitochondrial electron transport chain. Nature Structural & Molecular Biology **24**, 800–808, doi:10.1038/nsmb.3460 (2017).
52. Yan, B. *et al.* Membrane Damage during Ferroptosis Is Caused by Oxidation of Phospholipids Catalyzed by the Oxidoreductases POR and CYB5R1. *Molecular Cell* **81**, 355–369.e310, doi:https://doi.org/10.1016/j.molcel.2020.11.024 (2021).
53. Hope, M. J. & Cullis, P. R. Lipid asymmetry induced by transmembrane pH gradients in large unilamellar vesicles. Journal of Biological Chemistry **262**, 4360–4366, doi:https://doi.org/10.1016/S0021-9258(18)61356-0 (1987).
54. Hochberg, M. C. Updating the American College of Rheumatology revised criteria for the classification of systemic lupus erythematosus. Arthritis Rheum **40**, 1725, doi:10.1002/art.1780400928 (1997).
55. Petri, M. *et al.* Derivation and validation of the Systemic Lupus International Collaborating Clinics classification criteria for systemic lupus erythematosus. Arthritis Rheum **64**, 2677–2686, doi:10.1002/art.34473 (2012).

56. Aringer, M. *et al.* 2019 European League Against Rheumatism/American College of Rheumatology classification criteria for systemic lupus erythematosus. *Annals of the Rheumatic Diseases* **78**, 1151, doi:10.1136/annrheumdis-2018-214819 (2019).
57. Xie, C., Zhou, X. J., Liu, X. & Mohan, C. Enhanced susceptibility to end-organ disease in the lupus-facilitating NZW mouse strain. Arthritis Rheum **48**, 1080–1092, doi:10.1002/art.10887 (2003).
58. Bolte, S. & Cordelières, F. P. A guided tour into subcellular colocalization analysis in light microscopy. J Microsc **224**, 213–232, doi:10.1111/j.1365-2818.2006.01706.x (2006).

Figures

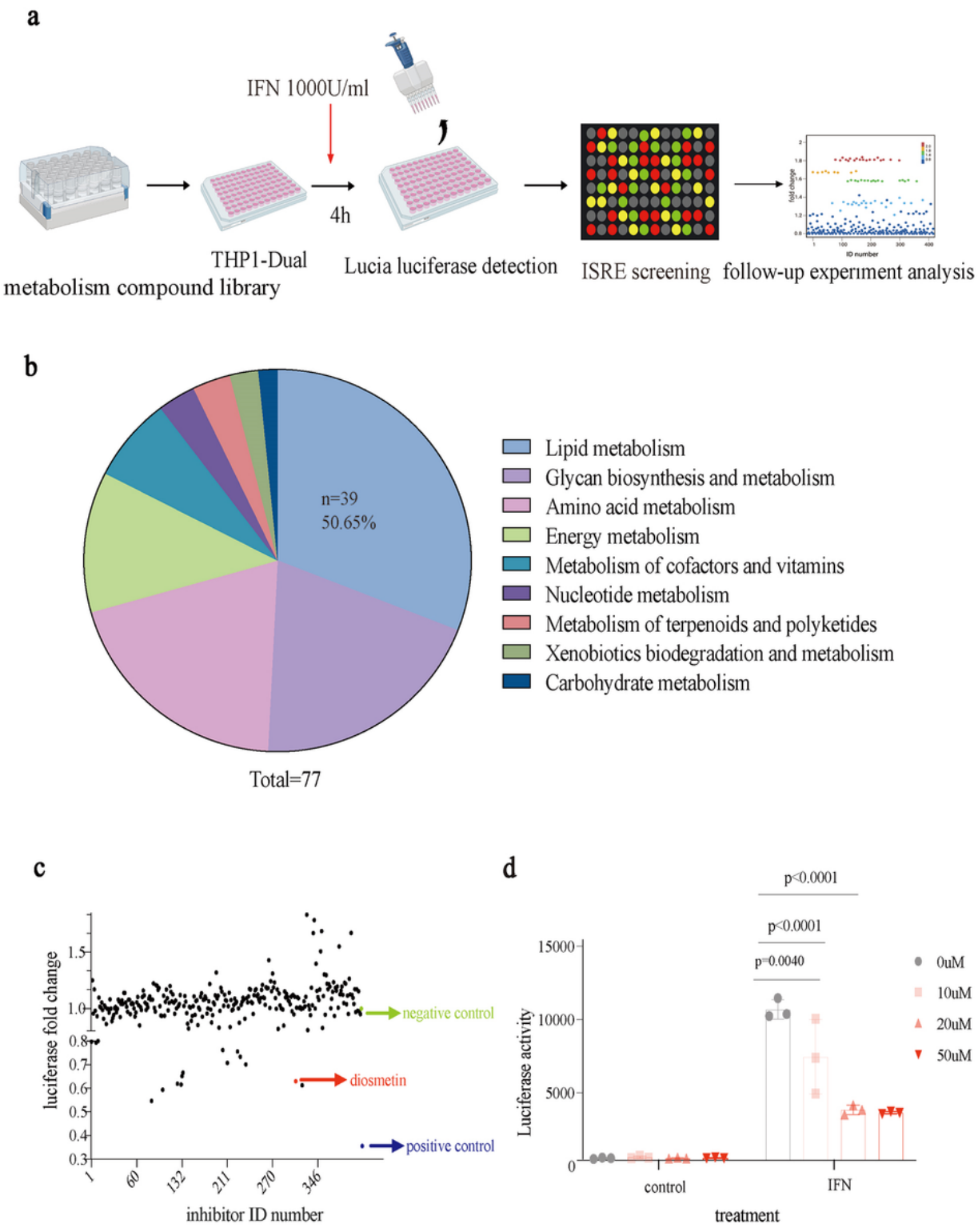

Figure 1

In vitro screening of metabolism compounds with THP1-Dual reporter cells. a.Diagram of screening strategy. **b.** Analysis of metabolic pathways of compounds. A total of 77 compounds negatively regulated type I IFN signaling, 50.56% (n=39) compounds act by lipid metabolism. **c**. A scatter plot of the inhibitory effects of all compounds. Cellular supernatant was collected for IRF response detection with QUANTI-Luc, and luciferase values were calculated to the negative control and GSK126 was as a positive

control. **d.** The effects of diosmetin with different concentrations on IFN-I signaling. THP1-Dual cells were incubated with Diosmetin (10uM, 20uM, 50uM) or vehicle for 30 minutes and then stimulated by 1000 U/ml IFN-I for 6 hours. Data in **d**are shown as mean ± SD and representative of 3 independent biological replicates, with P values calculated by a two-way ANOVA analysis. ns, P >0.05; *, P < 0.05; **, P < 0.01; ***, P < 0.005; ****, P < 0.0001.

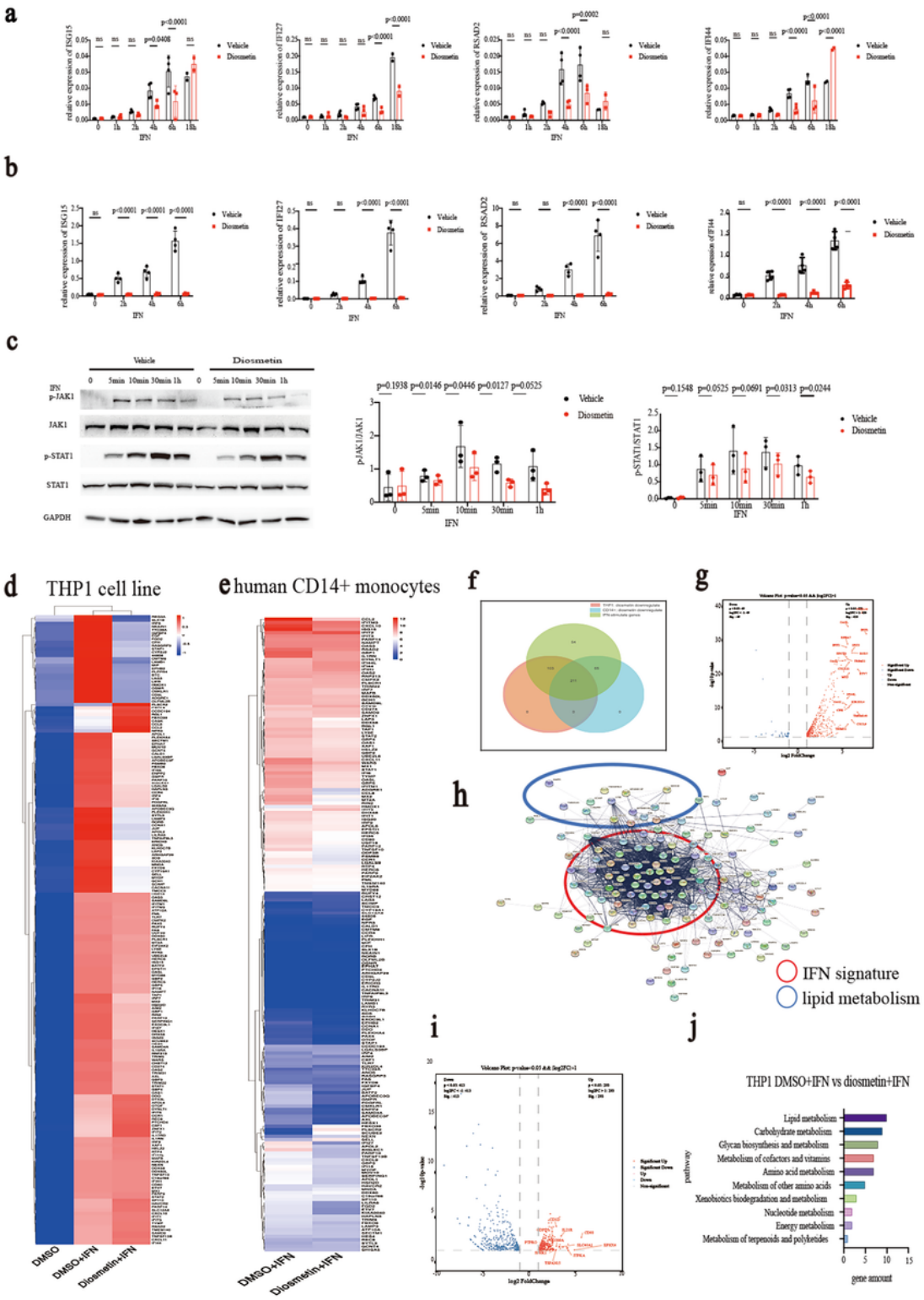

Figure 2

RNA-sequencing reveals diosmetin interplays with lipid metabolism during type I interferon signaling. a. THP-1 was incubated with diosmetin 50uM for 0.5 hours, then stimulated by IFN-I 1000U/ml for a time course. The expression of ISG15, IFI27, RSAD2, and IFI44 by RT-qPCR. **b.** CD14+ monocytes were isolated from PBMC, incubated with diosmetin 50uM for 0.5 hours, then stimulated by IFN-I 1000U/ml for a time course. The expression of ISG15, IFI27, RSAD2, and IFI44 by RT-qPCR. **c**. Left, western blotting in THP-1 cell line, THP-1 cells were incubated with diosmetin 50 uM or with the vehicle for 0.5 hours, then stimulated by IFN-I 1000U/ml for 5min, 10min, 30min, and 1h. Right, quantitative calculation of gray value by image J. **d.** Heatmap demonstration of differentially expressed genes (DEGs) in THP-1 cell lines. Differential expression of 193 genes with a 4-fold increase and a p-value less than 0.01 as IFN-I stimulation were demonstrated in the heatmap. **e.** Heatmap demonstration of differentially expressed genes (DEGs) in CD14+ monocytes. **f.** Venn diagram of ISGs that were regulated by diosmetin in THP-1 cell line and CD14+ monocytes. **g.** Volcanograms showed differential interferon-induced gene expression and lipid metabolism-associated genes in DMSO group and with IFN-I treatment group, volcanic map analysis was performed on gene clusters with a 2-fold change and a P value less than 0.05 in THP-1 cell line. **h.**Protein interaction network display a significant IFN signature and lipid metabolism between DMSO and DMSO+IFN in THP-1 cells. **i.** Volcanograms showed differential interferon-induced gene expression and lipid metabolism-associated genes in DMSO with IFN-I treatment and Diosmetin with IFN-I treatment group, volcanic map analysis was performed on gene clusters with a 2-fold change and a P value less than 0.05 in THP-1 cell line. **j.** Enrichment analysis of metabolic pathways in THP-1 cells treated in the presence or absence of diosmetin and stimulated by IFN-I. Data in **a, b** are shown as mean ± SD and representative of 4 independent biological replicates, with P values calculated by a two-way ANOVA analysis. Data in **c** are shown as mean ± SD and representative of 3 independent biological replicates, with P values calculated by a multiple paired t tests analysis. ns, P>0.05; *, P < 0.05; **, P < 0.01; ***, P < 0.005; ****, P < 0.0001.

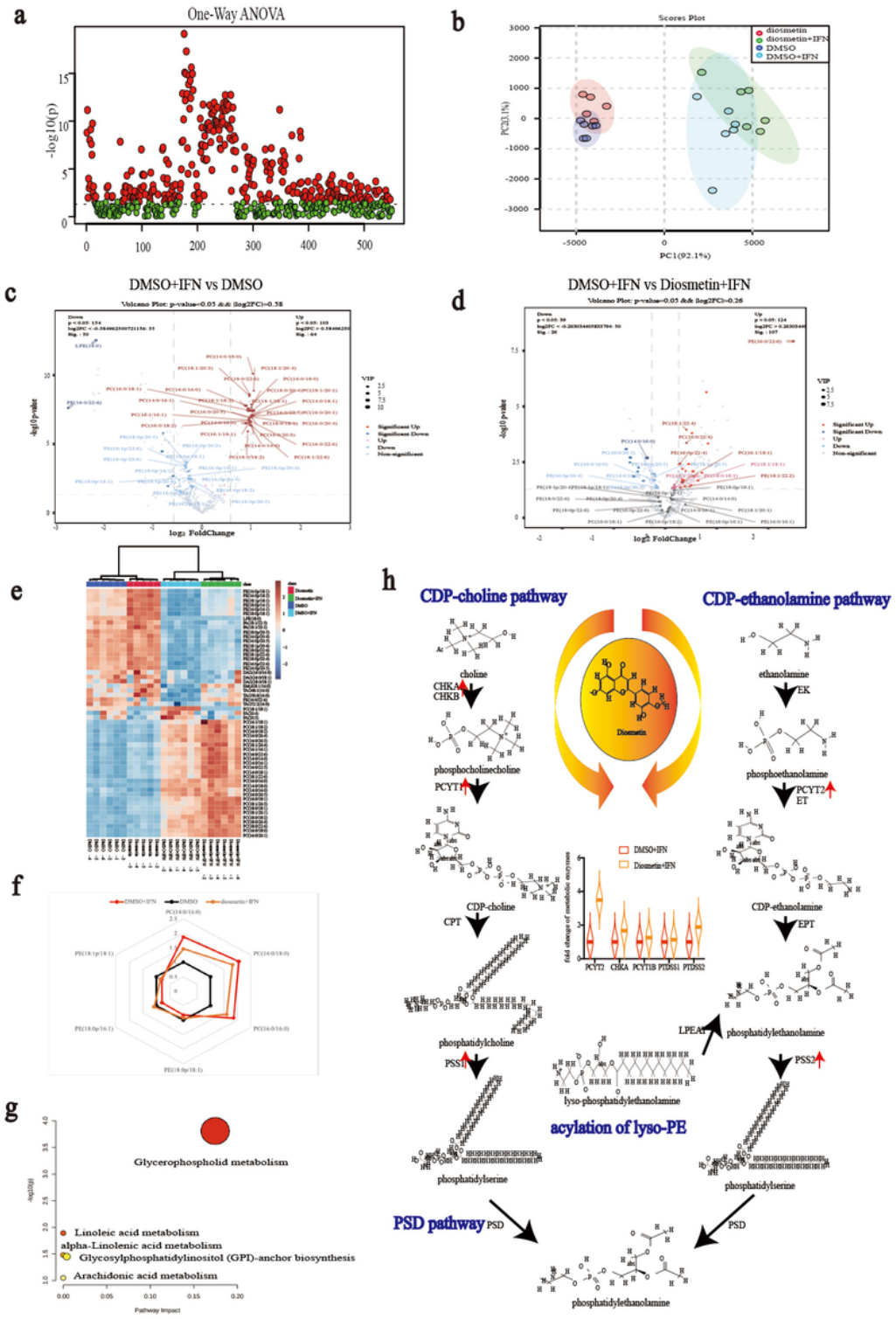

Figure 3

Lipid metabolic profiling reveals that diosmetin reduces the loss of PE during type I interferon signaling. **a.** The important metabolites in four groups were identified by ANOVA analysis. 403 significant compounds and 147 insignificant compounds were identified by ANOVA analysis. **b**. Partial Least Squares - Discriminant Analysis (PLS-DA). Samples can be well separated by different treatments. **c.** Volcanograms analysis of differential metabolites between DMSO with I-IFN stimulation and DMSO

groups. The red and blue dots showed the VIP sore was greater than 1 and fold change was greater than 1.5. Red dots were indicated to be higher in the DMSO with type I IFN stimulation, blue dots were indicated to be higher in the DMSO groups. **d**. Volcanograms analysis of differential metabolites between diosmetin with IFN-I stimulation and DMSO with type I IFN stimulation groups. The red and blue dots showed the VIP sore was greater than 1 and fold change was greater than 1.2. Red dots were indicated to be higher in the DMSO group, blue dots were indicated to be higher in the diosmetin group. Metabolites belonging to the phosphatidylethanolamine family and phosphatidylcholine family are marked. **e**. Heatmap of differential metabolites between four groups. **f**. Star symbol plots of mean data from DMSO, DMSO with type I IFN stimulation and diosmetin with type I IFN stimulation were drawn on the basis of the level of the six metabolites (PC (14:0/16:0), PC (14:0/18:0), PC (16:0/16:0), PE (18:0p/18:1), PE (18:0p/16:1), PE (18:1p/18:1)) after normalization to the corresponding DMSO mean values. **g**. Pathway enrichment analysis for these differential metabolites. **h**. Biosynthesis phosphatidylethanolamine (PE). After the synthesis of phosphoethanolamine (P-Etn) by ethanolamine (Etn) kinase (EK), PCYT2/CTP: phosphoethanolamine cytidylyltransferase (ET) catalyzed the conversion transformation of CTP and P-Etn into the activated nucleotide intermediate CDP-ethanolamine (CDP-Etn). Then the P-Etn moiety of CDP-Etn was transferred to the sn-3 hydroxyl of diacylglycerol by CDP-ethanolamine:1,2-diacylglycerol ethanolaminephosphotransferase (EPT). In the mitochondria-associated membranes (MAM), based exchange of PC, PE, and their corresponding plasmanyl-counterparts by PS synthase 1 and 2 (PSS1/2) yields PS and plasmanyl-PS, respectively. PS decarboxylase (PSD) that was located at the outer surface of the inner mitochondrial membrane can produce PE. CHKA, PCYT1, PCYT2, PSS1 and PSS2 are the key enzymes elevated by diosmetin treatment, which were marker red. The fold change expression of CHKA, PCYT1, PCYT2, PSS1 and PSS2 in diosmetin and IFN treatment group to DMSO and IFN treatment group are shown as violin plot. VIP, variable important in projection.

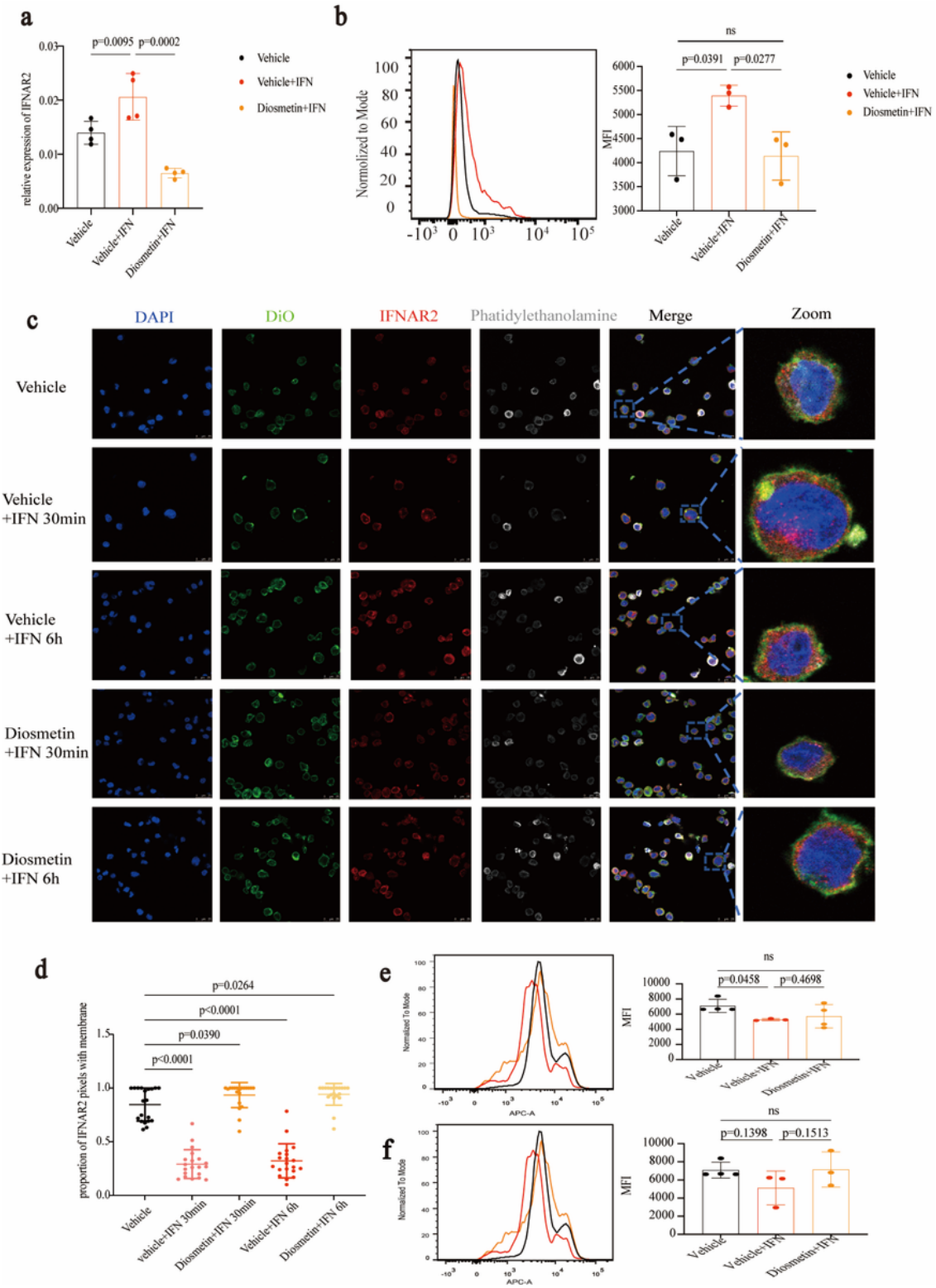

Figure 4

Diosmetin modulated the spatial signaling transducing process of type I IFN. a. RT-qPCR detection of IFNAR2. **b**. Flow cytometer analysis of IFNAR2. THP-1 cells were treated with vehicle or diosmetin for 30 minutes, then stimulated by type I IFN for 6 hours. Next, cells were collected and fixed for the following staining. **c.** Confocal images of DAPI, DIO, IFNAR2 and phatidylethanplamine of THP-1 cells in the activation of interferon and the effect of diosmetin. DIO was used to stain the plasma membrane. THP-1

cells were treated with vehicle or diosmetin for 30 minutes, then stimulated by type I IFN for 30 minutes or 6 hours. Next, cells were collected and fixed for the following staining. **d**. Quantification of co-localization of IFNAR2 and plasma membrane was by Mander's coefficient, indicating the proportion of plasma membrane containing IFNAR2 pixels. **e-f.** Flow cytometer analysis of phatidylethanolamine. THP-1 cells were treated with vehicle or diosmetin for 30 minutes, then stimulated by type I IFN for 30 minutes (**e**) and 6 hours (**f**). Next, cells were collected and fixed for the following staining. Scale bars, 25um. MFI, mean fluorescence intensity; **a, b, d, e, f,** are shown as mean ± SD with P values calculated by a two-way ANOVA analysis. **d**, n=20 cells, representative, per condition, data are shown as mean ± SD with P values calculated by a one-way ANOVA analysis. ns, P>0.05; *, P < 0.05; **, P < 0.01; ***, P < 0.005; ****, P < 0.0001.

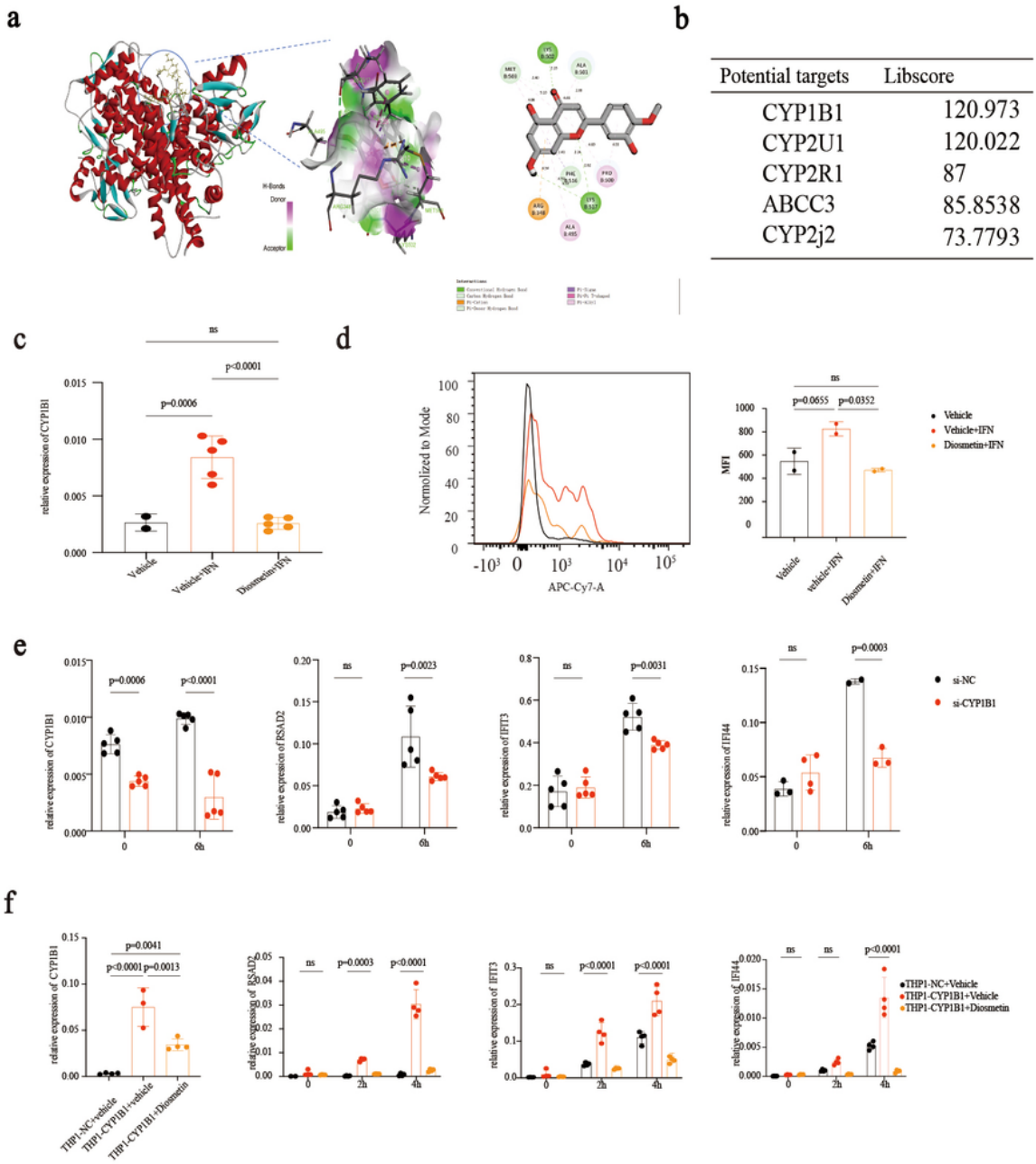

Figure 5

Molecular docking indicated diosmetin targeted to CYP1B1 at 6IQ5 site. **a**. 3D and 2D interactions between diosmetin and CYP1B1. Left, the crystal structure of CYP1B1 and the location of 6IQ5; Middle, Hydrophobic interaction between diosmetin and CYP1B1; Right, 2D interactions between diosmetin and CYP1B1. **b.** Libscores of five ligands. Different libscores were calculated by Biovia Discovery Studio 2019 to evaluate the docking models. **c**. RT-qPCR detection of CYP1B1. **d**. Flow cytometer analysis of CYP1B1.

THP-1 cells were treated with vehicle or diosmetin for 30 minutes, then stimulated by type I IFN for 6 hours. Next, cells were collected and fixed for the following staining. The mean fluorescence intensity (MFI) of CYP1B1 increased with interferon stimulation but decreased with diosmetin treatment. **e.**Knockdown the expression of CYP1B1 resulted in a decreased expression of interferon-stimulated genes. **f**. Detection of ISGs in lentivirus-stable THP-1 cells. Lentivirus-stable THP-1 cells were treated by vehicle or diosmetin for 30 minutes, then stimulated by IFN-I. Genes were detected by RT-qPCR. **c**,**d**, **e, f** are shown as mean ± SD and representative of repetitive biological replicates. Two-way ANOVA analysis (**c**,**d**) and one-way ANOVA analysis (**e**, **f**) were used to determine statistical significance. ns, P>0.05; *, P < 0.05; **, P < 0.01; ***, P < 0.005; ****, P < 0.0001.

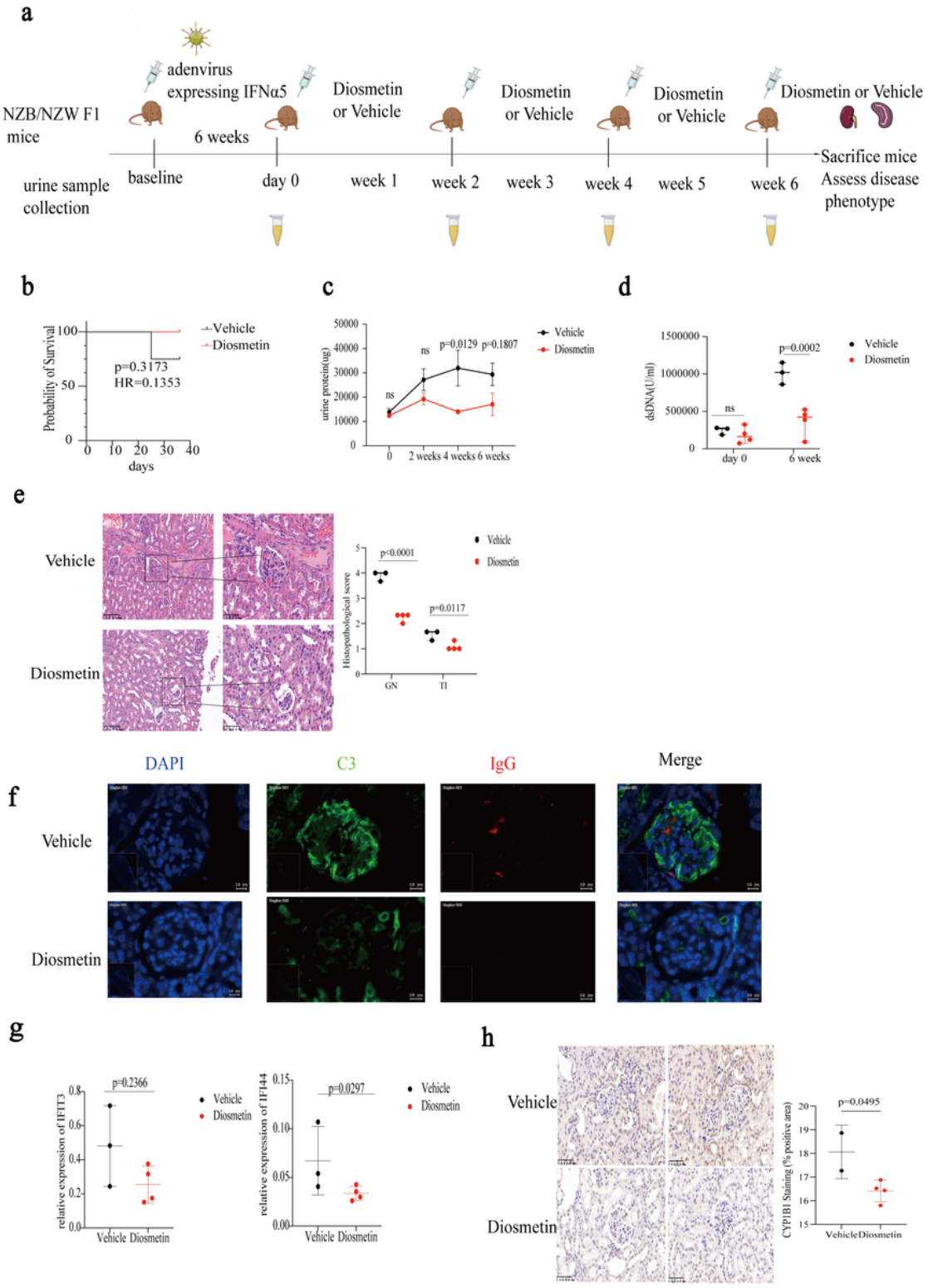

Figure 6

Therapeutic effects of diosmetin on interferon-mediated lupus of NZB/NZW F1 mice. a. Schematic of experimental procedures. 109 pfu of IFNa5-encoding adenovirus particles to NZB/NZW F1 mice of 6-week old (n=8), Diosmetin or vehicle was administrated intraperitoneally into two groups every other day for 6 weeks, and blood and urine are collected regularly for detection. **b.** Survival curve. **c**. Urine protein level. With time elapsed, total urine protein increased in the vehicle group (n=3) and diosmetin treatment

(n=4). **d.** Serum dsDNA levels. With time elapsed, serum dsDNA in the vehicle group (n=3) and diosmetin treatment (n=4). **e**. Hematoxylin and eosin (H&E) staining results. vehicle treatment (n=3), diosmetin treatment (n=4). Scale bar, 50um. **f**. Immunofluorescence of anti-mouse IgG2a and anti-mouse C3. n=3 in the vehicle group, n=4 in the diosmetin group. **g**. The expression of IFIT3 and IFI44 in the kidney. RT-qPCR was used to detect the expression of IFIT3 and IFI44 in vehicle group (n=3) and diosmetin treatment (n=4). **h**. Immunohistochemical staining of CYP1B1. vehicle treatment (n=2), diosmetin treatment (n=4). Scale bar, 50um. **c**, **d**, **e** and **g** are shown as mean ± SD, with P values calculated by a one-way ANOVA analysis. **b**was analyzed by curve compassion-Hazard Ratio (Mantel-Haenszel) model. ns, P>0.05; *, P < 0.05; **, P < 0.01; ***, P < 0.005; ****, P < 0.0001.

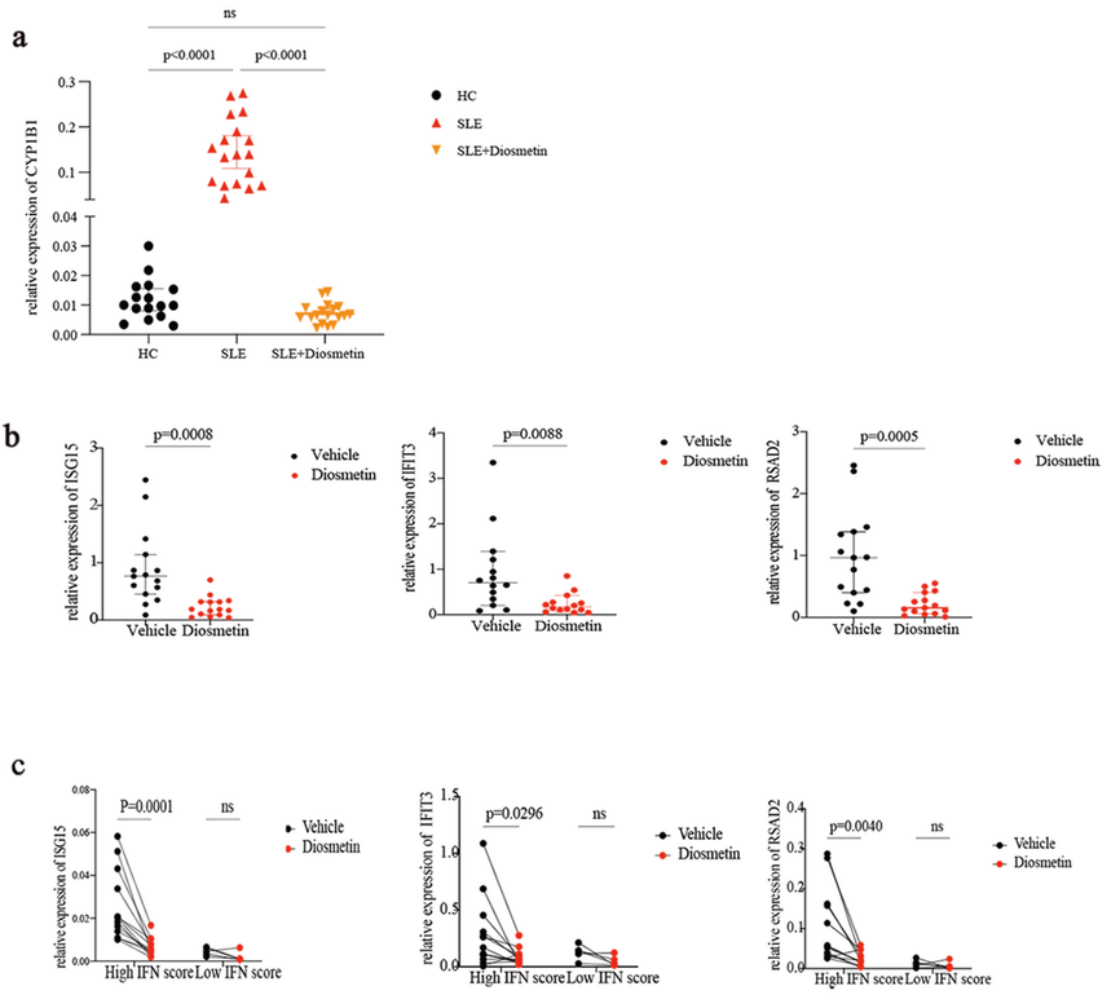

Figure 7

Diosmetin reduces "IFN SCORE" in SLE patients. a. The expression of CYP1B1 in PBMC of SLE. The expression of CYP1B1 in SLE patients (n=16), healthy control (n=16) and treatment with diosmetin 50 uM for 3 hours (n=16). **b.** Three ISGs expressions in PBMCs of SLE patients (n=18) (ISG15, IFIT3, and RSAD2) when treated with diosmetin or vehicle for 3 hours. **c.** Differential effects of drugs in patients with high and low interferon scores**.** Three ISGs (ISG15, IFIT3, and RSAD2) expressions in PBMCs of SLE

patients with high (n=13) and low IFN score(n=5). **a** and **b** are shown as mean ± SD. Ordinary one-way ANOVA (**a**), unpaired two-tailed t test (**b**) and two-way ANOVA analysis (**c**) were used to determine statistical significance. ns, P>0.05; *, P < 0.05; **, P < 0.01; ***, P < 0.005; ****, P < 0.0001.

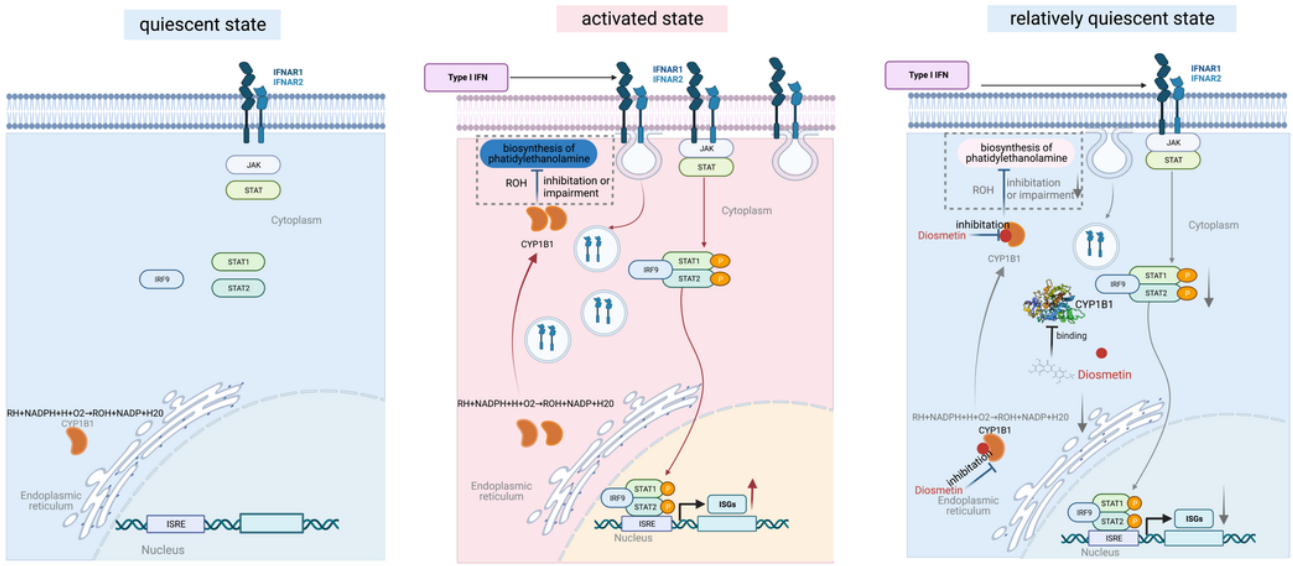

Figure 8

Model for the spatiotemporal control of IFNAR2 and JAK/STAT signaling by diosmetin. Left indicates the quiescent state of a cell. In the absence of type I IFN stimulation, the IFNAR complex is located on the plasma membrane and the pathway remains quiescent. Middle indicates the activated state of a cell. The formation of IFNAR1 and IFAR2 complex leads to the phosphorylation of the Janus family tyrosine kinases (JAKs), resulting in the recruitment and phosphorylation of signal transducer and activator of transcription (STAT) proteins. Together with IFN regulatory factor 9 (IRF9), and form complexes that translocate into the nucleus, and they act as transcription factors for IFN-induced genes. As an IFN-induced gene, CYP1B1, which results in the enzymatic reaction enhanced ($RH+NADPH+H+O_2=ROH+NADP+H_2O$), further results in the depletion of hydrogen ions and increased production of alkali in the cellular cytoplasm. The change of intracellular PH impaired the process of phosphatidylethanolamine biosynthesis. As a result, the decrease of phosphatidylethanolamine leads to the acceleration of IFNAR2 endocytosis. These changes ultimately further enhance type I IFN signaling. Right indicates the relatively quiescent state of a cell. Diosmetin entered the cytoplasm, first reducing the activity of the CYP1B1 by ligand-receptor binding, subsequently reduces the series of previous signal transduction. These changes ultimately stabilize changes in cell membrane and endocytosis of IFNAR2, further blunt type I IFN signaling.

Supplementary Files

This is a list of supplementary files associated with this preprint. Click to download.

- SupplementaryInfomation.docx